J. Micropalaeontology, 45, 159–175, 2026
https://doi.org/10.5194/jm-45-159-2026

Journal of Micropalaeontology
Open Access

Early Eocene evolutionary trajectories within the *Toweius* genus: insights from a newly identified species in the equatorial Atlantic

Joseph D. Asanbe and Jorijntje Henderiks

Department of Earth Sciences, Uppsala University, Uppsala, Sweden

Correspondence: Joseph D. Asanbe (joseph.asanbe@geo.uu.se)

Received: 11 November 2025 – Revised: 13 February 2026 – Accepted: 23 February 2026 – Published: 9 March 2026

Abstract. The genus *Toweius* was a globally prominent group of coccolithophores that thrived during the late Paleocene and early Eocene. Characterized by circular to elliptical coccoliths with three concentric tubes, *Toweius* is notable for its evolutionary linkage and abundance turnover with *Reticulofenestra* during the Early Eocene Climatic Optimum (EECO; 53–49 Ma). This study focuses on a newly identified *Toweius* morphotype (herein labeled *Toweius* type II) from the tropics, which lacks the typical inner and middle tubes found in known *Toweius* species (*Toweius* type I). The unique morphology of *Toweius* type II raises important questions about its origin and evolutionary significance. Biometric analysis of 1452 individual specimens, combined with light (LM) and scanning electron microscopy (SEM), reveals that coccolith size, central-area-to-rim ratio, and shape serve as reliable diagnostic criteria for distinguishing between morphotypes. Our results show that *Toweius* type II predominantly comprises small (∼ 3 µm) and thin (sub)circular coccoliths with a larger central area, lower mass estimate, and thus reduced calcification compared to *Toweius* type I. These distinctive traits, particularly the light calcification and a wider central area, may reflect a genetically regulated physiological adaptation that enabled *Toweius* type II to persist under extreme EECO conditions for an additional 2 million years following the decline of *Toweius* type I. Furthermore, the co-occurrence of this morphotype alongside rare transitional forms before the EECO suggests that it may not merely be an ecophenotypic response to environmental stress. Instead, we propose that *Toweius* type II evolved gradually through phyletic speciation, involving the complete loss of the inner R-unit tubes in a sub(circular) *Toweius* ancestor.

1 Introduction

Calcareous nannoplankton are calcifying, unicellular marine algae that have one of the most stratigraphically continuous and well-preserved fossil records among any group of organisms, dating back to the Triassic (e.g., Bown et al., 2004; Young et al., 2005). Because of their rapid evolutionary turnover, calcareous nannofossils are particularly useful for tracking paleoenvironmental changes and understanding how these changes drive evolutionary processes, including shifts in diversity and morphology (e.g., Haq and Lohmann, 1976; Wei and Wise, 1990; Bralower, 2002; Gibbs et al., 2006; Cappelli et al., 2019; Shepherd et al., 2021). A series of macroevolutionary changes in nannofossils have occurred in conjunction with global environmental change, such as the sharp decline in diversity during the Cretaceous/Paleogene mass extinction, followed by bursts of diversification throughout the Cenozoic, reaching peak diversity in the early Eocene (e.g., Bown et al., 2004).

Among the key nannofossil groups that dominated the late Paleocene and early Eocene was *Toweius* (Hay and Mohler, 1967), a placolith-bearing genus that originated in the Danian (∼ 63.6 Ma) with the evolution of small- to medium-sized, subcircular *Toweius pertusus* from *Prinsius* (Sullivan, 1965; Romein, 1979). The evolutionary history of *Toweius* during the middle to late Paleocene was marked by progressive morphological diversification, particularly in coccolith size, shape, central opening structure, and pore number (Romein, 1979; Bown et al., 2023). However, its relative abundance and diversity declined during the early Eocene, which was

characterized by major global warming episodes, particularly the Early Eocene Climatic Optimum (EECO; ∼53–49 Ma) (Mutterlose et al., 2007; Schneider et al., 2011; Self-Trail et al., 2012; Cappelli et al., 2019).

The EECO represents the warmest sustained global warming episode of the Cenozoic, characterized by elevated sea surface temperatures (SSTs; 10–14 °C increase; Westerhold et al., 2020), increased atmospheric CO_2 levels (exceeding 1000 ppmv; Hollis et al., 2009, 2019), a flattened meridional thermal gradient, and substantial alterations in marine biota (e.g., Zachos et al., 2001, 2008; Westerhold et al., 2018). This period marks a pivotal phase in nannofossil evolution, as *Toweius* underwent a permanent decline, ultimately being replaced by *Reticulofenestra* in what appears to be a major evolutionary transition (Agnini et al., 2006; Schneider et al., 2011; Cappelli et al., 2019; Alegret et al., 2021). The decline of *Toweius* has been linked to increasingly oligotrophic conditions and heat stress during the EECO (Schneider et al., 2011; Cappelli et al., 2019; Asanbe and Henderiks, 2025). The timing and patterns of this decline are not synchronous across latitudes. A recent study in the equatorial Atlantic (Ocean Drilling Project (ODP) Site 1258) suggests that the decline of *Toweius* occurred in two distinct phases across the EECO and was accompanied by the persistent presence of a newly observed *Toweius* morphotype, over a 2-million-year period following the decline of all known *Toweius* species (Asanbe and Henderiks, 2025). This discovery raises questions about the species-specific ecological tolerances of *Toweius* and the mechanisms driving its decline, particularly given the offset in the duration of the *Toweius*–*Reticulofenestra* turnover across latitudes.

This study integrates scanning electron microscopy (SEM), polarized light microscopy (LM), biometry, and statistical analysis to establish objective criteria to distinguish *Toweius* morphotypes across the EECO. While previous research has primarily focused on assemblage-level changes, this study takes a detailed morphological approach, examining phenotypic variability within *Toweius* and evaluating how paleoenvironmental conditions may have influenced morphotype selection during the EECO. Rather than focusing on species-level morphometric distinctions, this study considers *Toweius* as a single morphotype (*Toweius* type I) characterized by its distinctive V- and R-unit arrangements, typically forming three tube cycles with distinct optical properties (Nannotax; Young et al., 2003). This is then compared to the newly discovered *Toweius* morphotype (*Toweius* type II). Given the impact of dissolution on central area details, this study focuses on overall coccolith size, shape, and central opening size as primary diagnostic criteria.

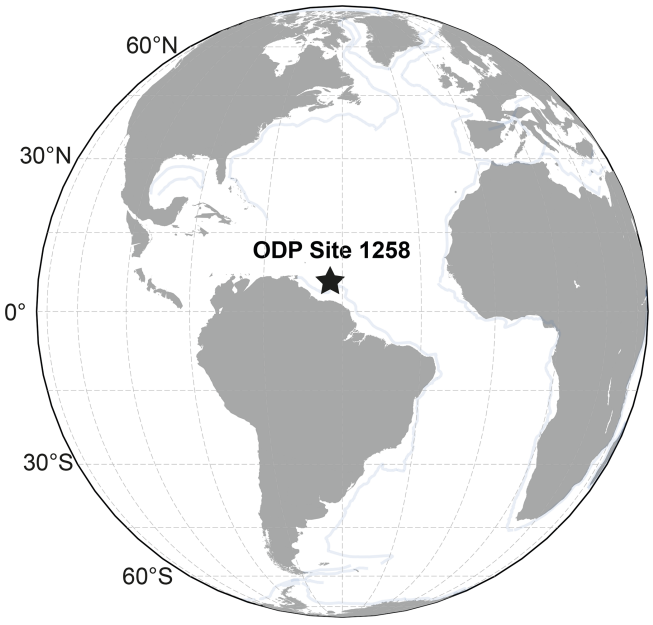

Figure 1. Early Eocene (50 Ma) paleogeographic reconstruction showing the location of ODP Site 1258. The plate tectonic reconstruction map was generated using GPlately1.0 (Mather et al., 2023) based on data from Müller et al. (2019).

2 Material and methods

2.1 ODP Site 1258

We analyzed 16 sediment samples from Ocean Drilling Project (ODP) Site 1258 located on the western slope of Demerara Rise, offshore Suriname (9°26′ N, 54°43.9′ W; at a water depth 3192 m below sea level (m b.s.l.); Erbacher et al., 2004; Müller et al., 2018, 2019). During the early Eocene (Fig. 1), the site location was closer to the Equator (paleocoordinates: 5°14′ N, 47° W; Müller et al., 2019), and sediments accumulated at a paleowater depth of ∼2500 m b.s.l. Samples were selected from between 68–100 revised meters composite depth (rmcd) in Holes 1258A and 1258B, within a ∼200 m thick unit of carbonate-rich (∼60 wt %) nannofossil chalk with foraminifers (Westerhold and Röhl, 2009), corresponding to the EECO. Calcareous nannofossils were abundant and well to moderately well preserved across the studied interval (Erbacher et al., 2004). Based on nannofossil census counts, including taxon-specific preservation indices (Asanbe and Henderiks, 2025), preservation is relatively consistent across the studied interval. Sample age estimates are based on an astronomically tuned age–depth model (Westerhold et al., 2017).

2.2 Sample preparation and coccolith imaging

Light microscopy slides were prepared following the "drop technique" (Bordiga et al., 2015) to guarantee an even distribution of coccoliths. LM images were captured using a polar-

izing microscope (Leica DM6000B, using an HCX PL APO 100x/1.47 objective and a pair of polarizer/analyzer or circular polarizer filters) equipped with a Hamamatsu ORCA-Flash 4.0 black and white digital camera (C11440; pixel resolution 0.064 µm). The images of *Toweius* specimens were taken both under cross-polarized (XPL) and circular-polarized (CPL) light for clear delineation of the outer- and inner-shield cycles. The combination of two circular polarizers (one left oriented and the other right oriented) and a green monochromatic light filter ($\lambda = 561$ nm; ZET561/10x, Chroma Technology) allows for the accurate measurement of calcite birefringence and coccolith thickness (Beaufort et al., 2021; see below). Regarding *Toweius* structural architecture, the R units form the bright middle and inner tubes as well as the lower part of the proximal shield, while the outermost tube, distal shield, and upper part of the proximal shield are primarily made up of V units (Fig. 2; Young et al., 2003). These architectural elements impart distinctive optical properties to *Toweius* coccoliths under XPL, where dark outer and bright inner cycles are visible. Such unique birefringence patterns facilitate species/morphotype taxonomic determination based on coccolith morphology.

For scanning electron microscopy (SEM), a small amount of sample was suspended in a 0.2 M ammonia solution (pH $\approx$ 11.3; cf. Bordiga et al., 2015) and was dropped onto a cover glass, mounted on a stub with carbon tape, and dried before sputtering with gold-platinum alloy prior to analysis. SEM imaging of nannofossil specimens was conducted at the Department of Earth Sciences, Uppsala University, using a high-vacuum Zeiss Supra 35VP field emission SEM equipped with a VPSE low-vacuum detector. Images were captured using a 20 kV accelerating voltage, a 30.0 µm aperture, and an average working distance of $\sim$ 6 mm.

2.3 Coccolith biometry

All biometric measurements were conducted on CPL images using a manual setup within the SYRACO software (Beaufort et al., 2014; with CPL upgrades as described in Beaufort et al., 2021). Specimens were selected from live images by drawing a region of interest (ROI). The combination of left-oriented and right-oriented CPL settings results in a composite, 8-bit gray-scale image (CP-CPI) that is segmented (by manually setting a gray level (GL) threshold), analyzed, and saved. The measured parameters include the entire coccolith and central opening dimensions, such as length and width. The SYRACO software automatically measures coccolith area (µm^2), mean thickness (µm; as derived from mean GL), and calcite mass, following the principle of linear correlation of calcite birefringence (brightness) to coccolith thickness (Beaufort, 2005; Beaufort et al., 2014, 2021). Theoretically, using monochromatic green light ($\lambda = 561$ nm), thickness can be determined for specimens between 0 and 1.63 µm thick (Beaufort et al., 2021; Sect. S1 in the Supplement). The latter relationship is only true for R units that have their crystallographic orientation parallel to the glass slide, whereas equally thick V units appear only slightly birefringent under CPL and thus result in a systematic underestimation of calcite mass (Fig. 2; Cubillos et al., 2012; Šupraha and Henderiks, 2020). Yet, mean GL-derived thickness and mass indices still serve as accurate, relative comparisons between morphotypes (intra-specific variability).

V units also make detecting the distal shield edges of *Toweius* placoliths somewhat challenging, since their GLs are close to background GL ("black") under CPL. To optimize segmentation, the lower threshold was set to GL = 22 for small specimens (type II) and GL = 27 for larger specimens (type I). The threshold was further refined to clearly delineate the coccolith outer margin and central area from the background, particularly in clouded samples. For mean thickness and mass index considerations, this implies a slight underestimation for the larger specimens (since the threshold value is subtracted before mean GL is calculated for the segmented specimen), but we consider this bias negligible in the context of the effect of generally larger sizes and the presence of additional R-unit cycles in type I (Fig. 2). Additional shape parameters, independent of size, were calculated. The ratio of the central area to rim width (CA / rim) assesses the relative proportion of central area length to the rim width. Coccolith circularity was calculated following (e.g., Henderiks, 2008)

$$\text{Circularity index} = \sqrt{\frac{W}{L}}, \quad (1)$$

where L is coccolith length (maximum diameter), and W is coccolith width (minimum diameter). A high circularity index refers to a more circular shape, while lower circularity indicates a more elliptical coccolith shape. The frequency distribution and cross plots of the different measured and calculated parameters were compared to obtain first-hand morphometric criteria that distinguish the main *Toweius* morphotypes. For each morphotype, if present, a minimum of 50 specimens were measured per sample. In total, 1452 specimens were measured, including 610 *Toweius* type I and 842 *Toweius* type II. Three additional samples were selected from the depth interval below the EECO to investigate the stratigraphic range of *Toweius* type II and any possible "transitional" forms (no biometry performed).

A subset of original images measured using the aforementioned methodology were re-evaluated with a fixed threshold (GL = 25) applied to both *Toweius* type I and *Toweius* type II. In total, 599 images (334 *Toweius* type I and 266 *Toweius* type II) from 11 samples in which both morphotypes co-occur were re-analyzed as a batch using a custom-made macro in Fiji software (ImageJ v2.16.0). The software determined GL ranging from 0 (black) to 255 (white) and performed size measurements (area, perimeter, length, and width of the fitted ellipse) on coccolith objects. Although central area dimensions were not determined with this approach, re-evaluation was necessary to validate relative differences in coccolith size, mean thickness, and mass index

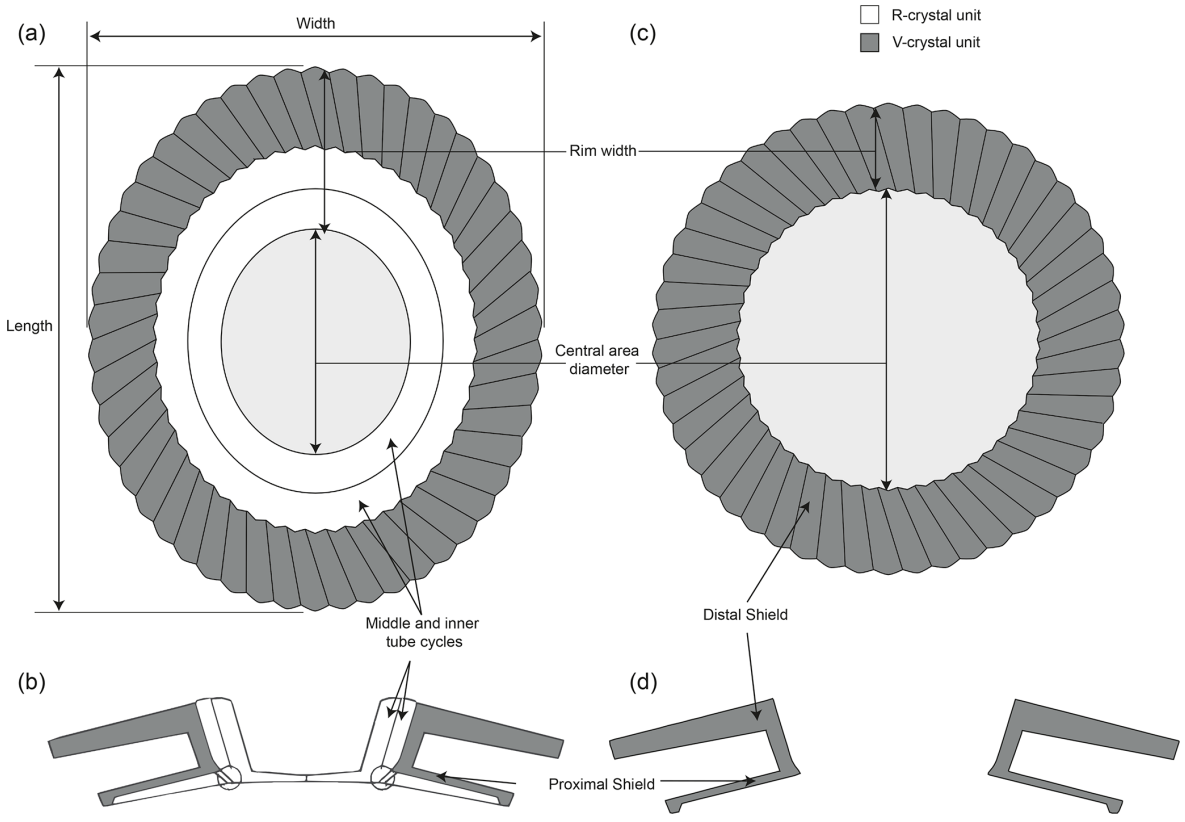

Figure 2. Structural morphology of *Toweius* and measured parameters. **(a–b)** A schematic distal view and cross-section V–R model of *Toweius* type I and **(c–d)** type II. The V–R model is based on Young et al. (2003). Only R units appear fully birefringent under CPL because their *c*-axis orientation is parallel to the plane of observation when a coccolith lies flat on the glass slide.

using a consistent thresholding approach (see Sects. S1–S2 and Figs. S1–S4 in the Supplement). Coccolith thickness and mass were estimated following the protocol described in Beaufort et al. (2021):

$$d = \mathrm{MGL} \cdot \left(\frac{1.63}{256}\right) (\mu\mathrm{m}) \quad (2)$$

$$\rho\mathrm{mass} = d \cdot A \cdot (\mathrm{pg}), \quad (3)$$

where d is the mean thickness, MGL is the mean gray level, A is the area of the coccolith in μm^2, and ρ is the density of calcite ($2.71\ \mathrm{pg}\,\mu\mathrm{m}^{-3}$).

3 Results

3.1 *Toweius* morphological and crystallographic description

The XPL, CPL, and SEM images of *Toweius* types I and II are presented in Plates 1 and 2. These images provide a detailed visual comparison of the morphological and crystallographic characteristics distinguishing the two groups. All coccoliths belonging to *Toweius* type I display a highly birefringent inner-shield cycle (tube cycle) and a low-birefringent (dark gray) outer-shield cycle under LM (Plate 1, figs. 1–2). SEM observations show that the coccolith architecture features three distinct concentric tube layers (Plate 1, figs. 3–8). Specifically, the distal side of the coccolith is characterized by the extension of the inner- and middle-tube cycles (R unit), while the proximal shield surface is covered by a layer of coccolith elements (R unit) (Plate 1, figs. 3–8). *Toweius* type II coccoliths show subcircular to circular outlines and wide-open central areas. Under LM, these specimens exhibit faint birefringence and a predominantly dark appearance (Plate 2, figs. 1–6). A distinguishing feature of this morphotype is the presence of two prominent lens-shaped extinction features along the rim, which appear curly when the focus is adjusted (Plate 2, figs. 1–6). These curved extinction points are partially occluded by the bright inner-tube cycle elements in *Toweius* type I (Plate 1, figs. 1–2). SEM observations of *Toweius* type II reveal coccoliths that have intact proximal and distal shields but are composed of a single tube cycle element, notably lacking the R-unit element from both the distal and the proximal views (Plate 2, figs. 7–14). Nonetheless, the crystallographic characteristics of *Toweius* type II distal shields closely resemble those of *Toweius* type I. Specifically, the distal shield elements exhibit a sinistral obliquity, and the crystal edges between the rhombohedral faces in both *Toweius* type I and *Toweius* type

II follow similar orientation of the crystallographic *a* and *c* axes (compare Plate 1, figs. 3–8, and Plate 2, figs. 7–14).

3.2 Biometry and statistical analyses

The comparison between the primary dataset and validation dataset is presented and described in the Supplement (see Sect. S2 and Figs. S3–S4 in the Supplement). It is important to note that the entirety of the biometry and statistical analyses presented and described in the main text is based on the full primary dataset. The morphometric analysis reveals a bimodal distribution in coccolith size (length) for the entire dataset encompassing *Toweius* types I and II ($N = 1452$), with overall coccolith size (length) ranging from 2.08 to 7.23 µm (Fig. 3a). Coccoliths belonging to *Toweius* type I exhibit a wider size variation, ranging from 2.22 to 7.23 µm (mean = 4.14 µm), than *Toweius* type II, which spans 2.08 to 4.41 µm (mean = 2.73 µm) (Fig. 3a). The smaller-sized *Toweius* type I coccoliths (< 4 µm) and *Toweius* type II substantially overlap, ranging from 2.21–4.41 µm. The majority of *Toweius* type II has size ranges centered between 2 and 3 µm. The circularity index shows that all measured coccoliths range from elliptical (0.80) to perfectly circular (1) (Fig. 3b). Although there is a substantial overlap in the degree of circularity between the two morphotypes, *Toweius* type II is generally more circular (mean = 0.95) compared to *Toweius* type I (mean = 0.91) (Fig. 3a).

The density distribution and cross plot of the width, CA / rim ratio, mean thickness, and mass index against length reveal two distributions within the dataset. Compared to coccolith length and circularity distribution, these parameters distinctly delineate between *Toweius* types I and II, with very little overlap (Fig. 3c–f). Specifically, the CA / rim ratio of *Toweius* type I ranges from 0.05 to 2.81 (mean = 0.63), with the majority of the observations falling well below 1 (Fig. 3d). In contrast, *Toweius* type II displays a high degree of variability in CA / rim ratio values, ranging between ∼ 0.05 and 6.66 (mean = 2.63). The CA / rim ratio in this morphotype is inversely correlated with coccolith length, whereas the CA / rim ratio of *Toweius* type I is relatively stable across specimens of different sizes (Fig. 3d). Furthermore, coccolith mean thickness and mass index derived from coccolith birefringence (GL) show a strong positive correlation with overall coccolith size (length), with correlation coefficients of $r = 0.85$ and $r = 0.84$, respectively (Fig. 3e–f). The mean coccolith thickness and mass index of *Toweius* type I reach maximum estimates of 0.77 µm (mean = 0.38 µm) and 71.67 pg (mean = 10.81 pg). In contrast, *Toweius* type II coccoliths are relatively much thinner and lightly calcified, with mean thickness and mass index ranging from 0.14 to 0.37 µm (mean = 0.22 µm) and 0.70 to 10.72 pg (mean = 2.11 pg), respectively (Fig. 3e–f).

3.3 Descriptive statistics and significance difference test

Box-and-whisker plots illustrate the median, interquartile range, overall spread, and symmetry of the morphometric dataset (Fig. 4). The results reveal a clear distinction between the two *Toweius* morphotypes across all major morphometric parameters, particularly within the interquartile range (25th–75th percentile) (Fig. 4). A Shapiro–Wilk normality test indicates that the morphometric parameters do not follow a normal distribution. Since the distribution might only be slightly skewed, we applied both parametric and non-parametric statistical methods to rigorously assess differences between *Toweius* morphotypes. The two-sample *t* test and Mann–Whitney test confirm that *Toweius* type I differs significantly from *Toweius* type II in length, circularity, CA / rim ratio, and thickness (Table 1).

4 Discussion

4.1 *Toweius* morphotype comparison and taxonomic implications

Previous studies (e.g., Bown, 2010; Self-Trail et al., 2012) have highlighted that the size and central area structural variability in *Toweius* likely reflect a greater number of biological species than are currently recognized by morphological criteria. Such subtle differences parallel the diversity observed in modern *Reticulofenestra* lineages, including *Emiliania huxleyi* and *Gephyrocapsa*. Therefore, the wide variation in shape and size among coccoliths classified as *Toweius* type I reflects the pooling of multiple formally defined *Toweius* species into a single morphotype (Fig. 3a). The key unifying feature in this morphotype is the presence of a birefringent (R-unit) inner-tube cycle and a darker (V-unit) outer tube, genus-level diagnostic criteria that distinguish *Toweius* type I from *Toweius* type II (Fig. 3a). *Toweius* type II lacks the inner-tube cycle (R unit) associated with *Toweius* and can be further differentiated by its small (∼ 3 µm) and (sub)circular to circular coccoliths with a wide central opening (CA / rim ratio > 1) (Fig. 3a, b).

Although previous studies (Bown and Pearson, 2009; Gibbs et al., 2018) have reported small, fragile *Toweius* species comparable to *Toweius* type II in terms of size, it is important to note that these morphotypes still retain the complete *Toweius* coccolith architecture, making them distinct from *Toweius* type II. Bralower and Mutterlose (1995) documented the occurrence of *Toweius* specimens at ODP Site 865 in the tropical Pacific, which were, at the time, interpreted as severely etched *Toweius* shields. Detailed reanalyses of Site 865 samples (Asanbe and Henderiks, 2025) revealed consistencies between the *Toweius* type II specimens described in this study and those previously observed in the equatorial Pacific (Bralower and Mutterlose, 1995). Notably, *Toweius* type II is more abundant at Site 1258, where carbonate preservation is better than at Site 865, where there

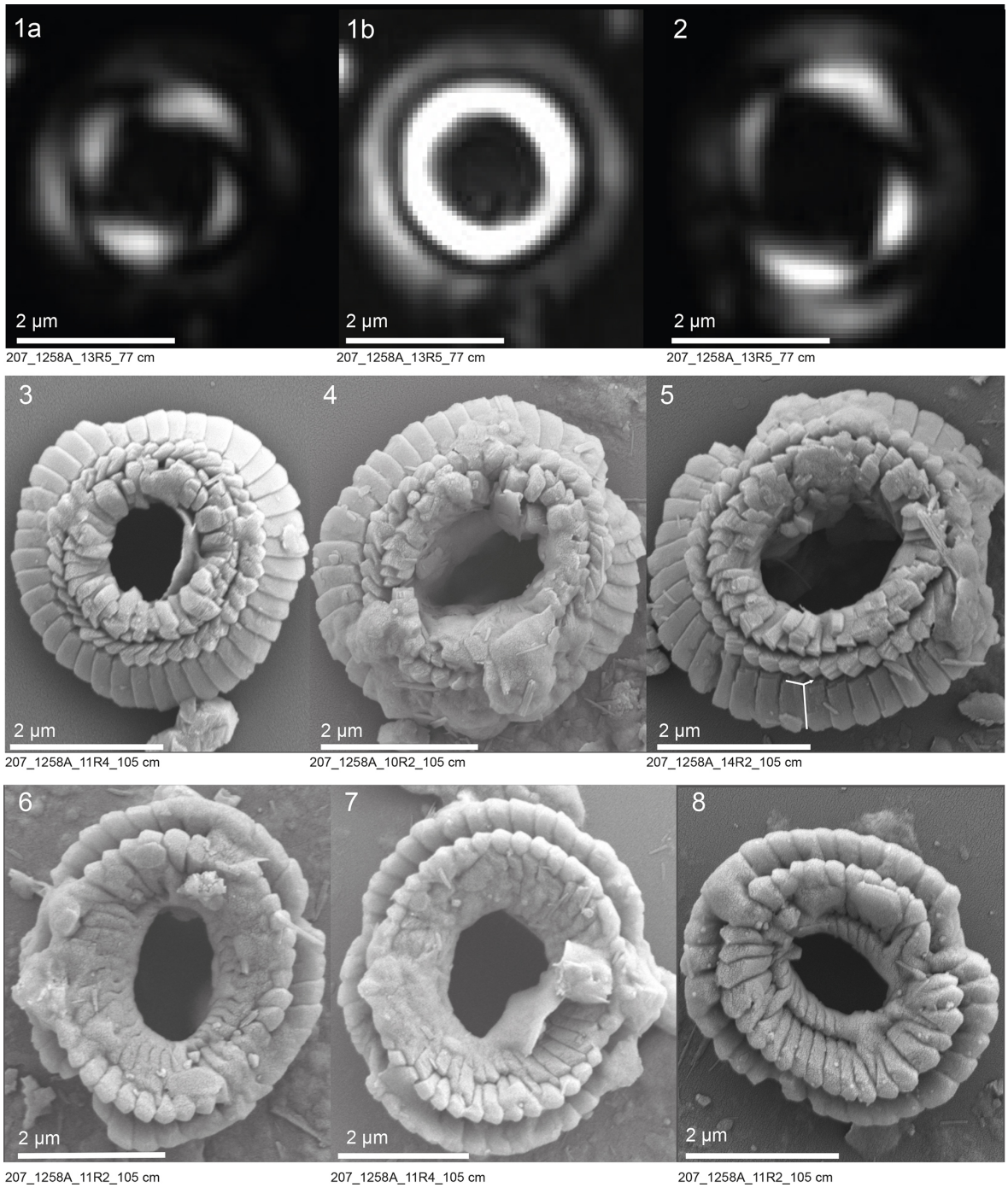

Plate 1. Polarized microscopy (XPL, CPL) and SEM images of *Toweius* type I. **(1–2)** Images of specimens under XPL and CPL. **(3–5)** Distal views and **(6–8)** proximal views of specimens under SEM. The "Y"-shaped annotation in fig. **(5)** (compare with Plate 2, fig. 10) indicates similarities in calcite crystal orientation in *Toweius* types I and II specimens. Scale bars equal 2 µm.

is indeed evidence of more severe dissolution (Asanbe and Henderiks, 2025). The temporal consistency in the abundance of this morphotype at both tropical sites, along with its distinct morphometric characteristics revealed in this study, supports the interpretation that *Toweius* type II represents a truly distinct species (or group of species) (Fig. 5b).

Despite the absence of an R unit, other structural similarities, such as the sinistral obliquity of the distal shield elements, the curly extinction pattern on the outer-tube cycle (compare Plate 1, figs. 1–2, with Plate 2, figs. 1–6), and the orientation of the V units (compare Plate 1, figs. 3–8, with Plate 2, figs. 7–14), provide strong support for the

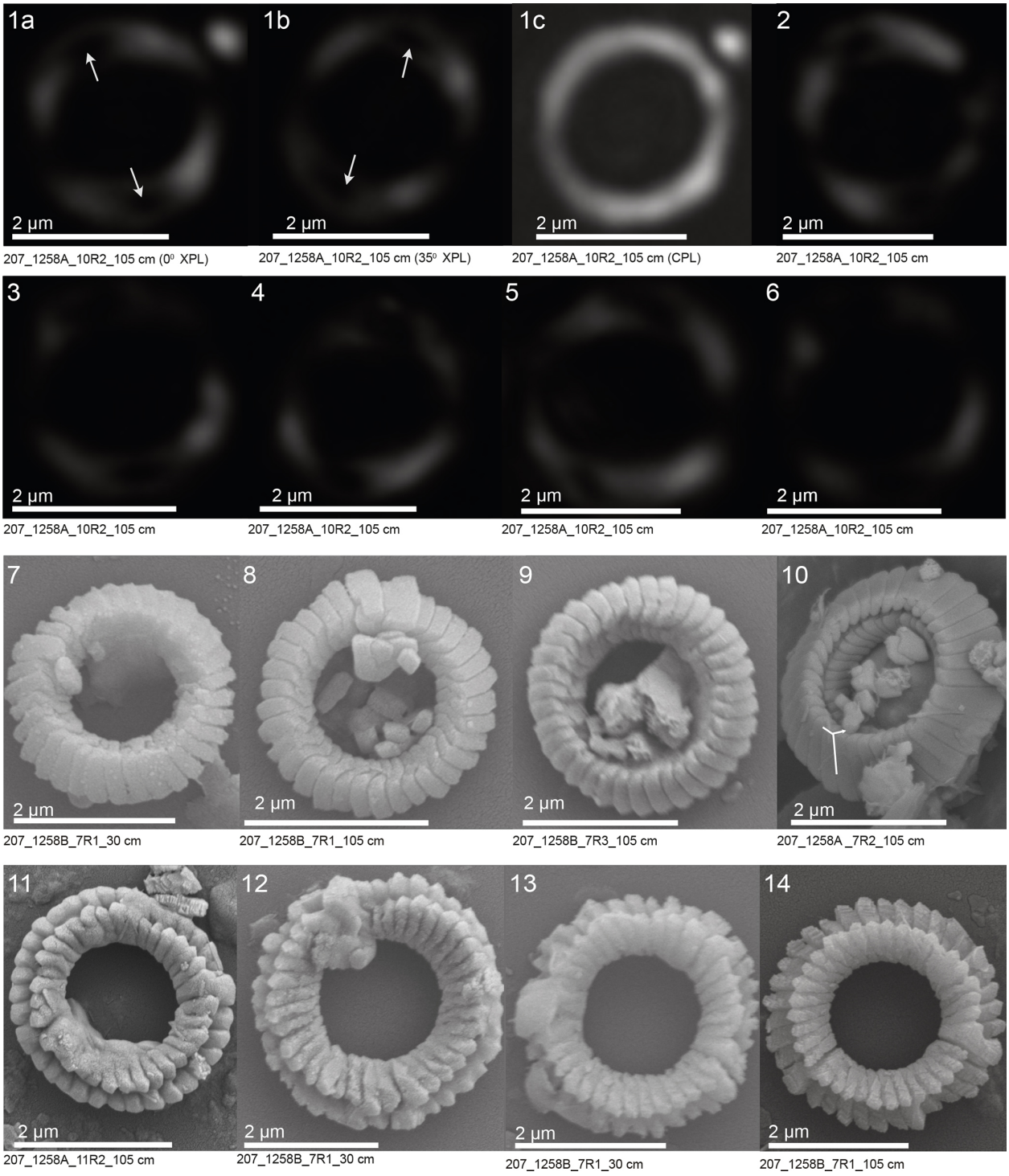

Plate 2. Polarized microscopy (XPL, CPL) and SEM images of *Toweius* type II. **(1)** Holotype specimen under XPL (at 0 and 35°) and CPL (see formal species description in the Appendix). **(2–6)** Additional specimens of *Toweius* type II under XPL. **(7–10)** Distal views and **(11–14)** proximal views of specimens under SEM. White arrows in figs. **(1a)** and **(1b)** highlight the characteristic, curved ("curly") lens-shaped extinction features along the coccolith rim, also visible in figs. **(2)**–**(6)**. The "Y"-shaped annotation in fig. **(10)** (compare with Plate 1, fig. 8) indicates similarities in calcite crystal orientation in *Toweius* types I and II specimens. Scale bars equal 2 µm.

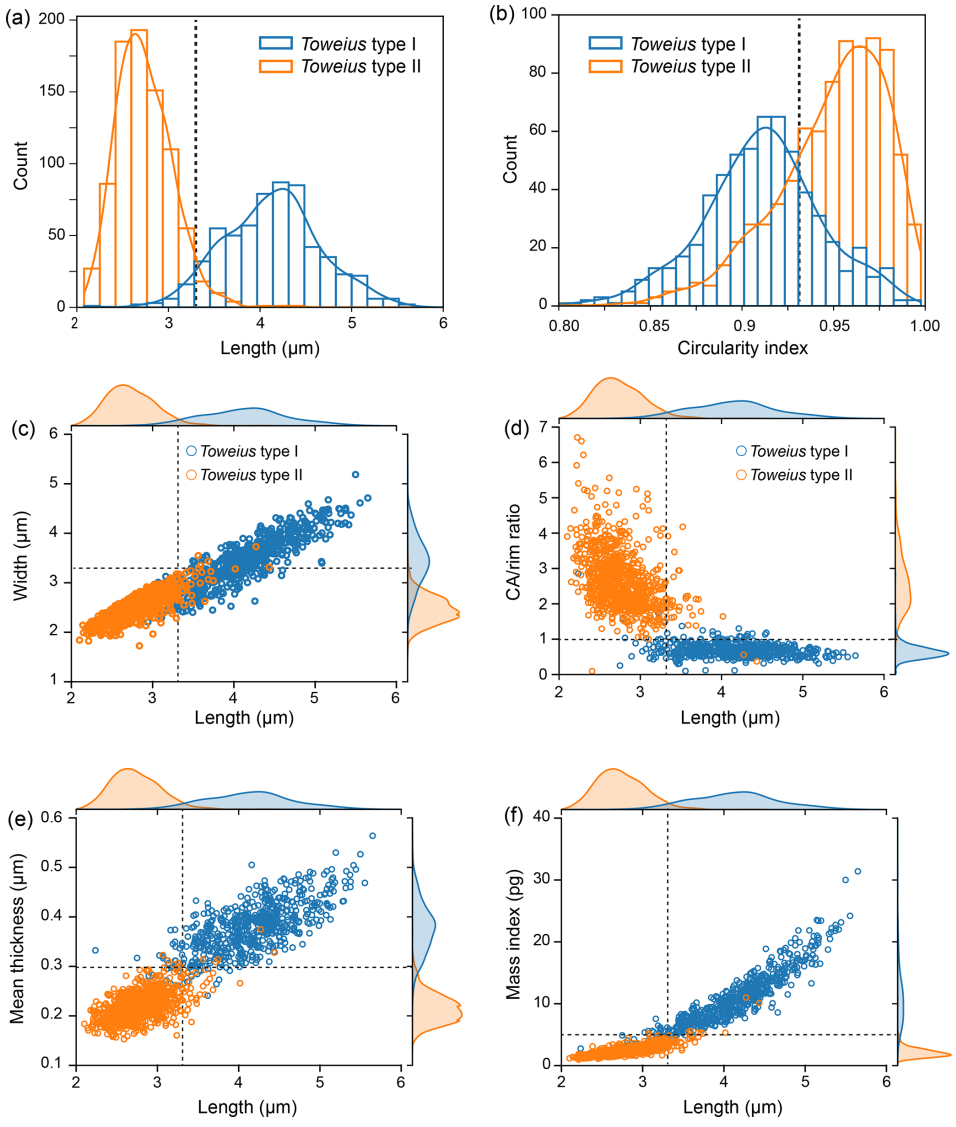

Figure 3. Histogram distribution and cross plots of the measured morphometric parameters distinguishing *Toweius* morphotypes. **(a)** Histogram with normal distribution fit of coccolith length and **(b)** circularity. **(c)** Cross plots and density curves of coccolith length against width, **(d)** CA / rim ratio, **(e)** mean thickness (based on mean GL), and **(f)** mass index. $N = 610$ (type I) and $N = 842$ (type II).

Table 1. Summary of statistical tests comparing biometric parameters between *Toweius* type I and type II coccoliths. Reported values are p values for each test, with Monte Carlo permutation p values in parentheses (in all cases = 0.0001), showing the robustness of observed differences.

Parameters tested	T test (for equal means)	Mann–Whitney test (for equal medians)
Length	0 (0.0001)	1.121×10^{-221} (0.0001)
Width	6.403×10^{-128} (0.0001)	1.212×10^{-111} (0.0001)
CA / rim	0 (0.0001)	2.649×10^{-228} (0.0001)
Circularity index	2.675×10^{-311} (0.0001)	1.039×10^{-194} (0.0001)
Mean thickness	0 (0.0001)	9.799×10^{-230} (0.0001)

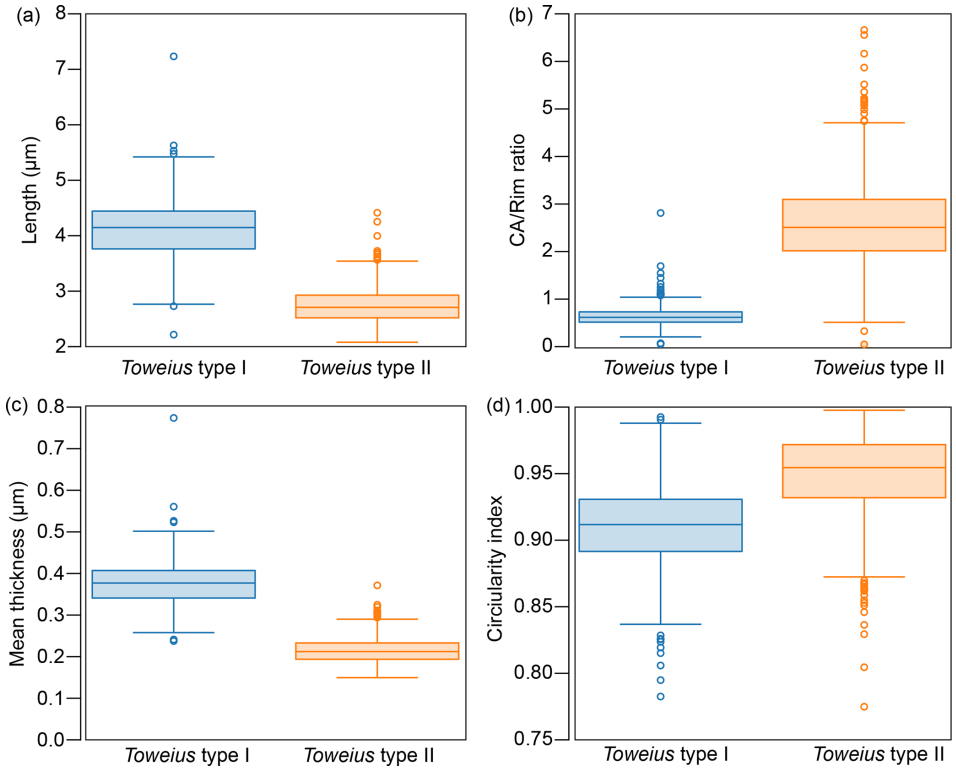

Figure 4. Boxplot of coccolith **(a)** length, **(b)** CA / rim ratio, **(c)** mean thickness, and **(d)** rim of *Toweius* morphotypes. The shaded box shows the 25th and 75th percentile distribution, while the circle denotes outliers in the dataset. $N = 610$ (type I) and $N = 842$ (type II).

taxonomic (and phylogenetic) placement of *Toweius* type II within the *Toweius* genus. The (sub)circular coccolith shape of *Toweius* type II suggests that it may be related to *Toweius* species with similar morphology. Among all known *Toweius* species, *Toweius rotundus* exhibits the greatest resemblance to *Toweius* type II in terms of size and shape. While *T. rotundus* was initially reported to have gone extinct during the PETM at Tanzania Drilling Project (TDP) sites (Bown and Pearson, 2009), later studies identified its presence above its previously assumed extinction level (Schneider et al., 2011; Shamrock and Watkins, 2012).

The overlapping stratigraphic ranges of *Toweius* type II and *T. rotundus* suggest a possible phylogenetic relationship. It is plausible that *T. rotundus* underwent substantial morphological modifications in tropical environments, including a reduction in or complete loss of the R unit. The precise mechanisms underlying these morphological differences remain unclear. Therefore, we need to assess whether *Toweius* type II resulted from selective dissolution, represents a case of malformation, or constitutes a true evolutionary lineage derived from *T. rotundus*. Below, we explore these possibilities by examining the potential roles of preservation conditions, ecological factors, and phyletic speciation in the emergence of *Toweius* type II prior to the EECO.

4.2 Disentangling macroevolutionary signal from preservation bias

Episodes of extreme global warming, such as the EECO, are typically associated with major shifts in carbonate preservation due to the complex interplay between elevated atmospheric CO_2 levels, ocean acidification, lysocline dynamics, and CCD shoaling (e.g., Agnini et al., 2007; Dunkley Jones et al., 2008; Pearson et al., 2008; Raffi and De Bernardi, 2008). Carbonate dissolution can significantly alter the taxonomic composition of calcareous nannofossil assemblages by selectively removing fragile structures, often resulting in the complete loss of small and delicate taxa while rendering larger ones unidentifiable (Roth and Thierstein, 1972; Roth, 1978; Bown et al., 2008). The impact of a preservation bias in our study can be considered from two perspectives: (1) as a potential source of bias in morphometric data due to etching and overgrowth and (2) as a possible mechanism underlying morphological differences between the two *Toweius* morphotypes.

Previous studies at Site 1258 indicate that carbonate preservation remained relatively stable throughout the EECO (Fig. 5a; Asanbe and Henderiks, 2025). SEM evidence reveals a moderate and uniform degree of etching in delicate central area structures and minimal overgrowth in most *Toweius* specimens. Central area etching, in particular, com-

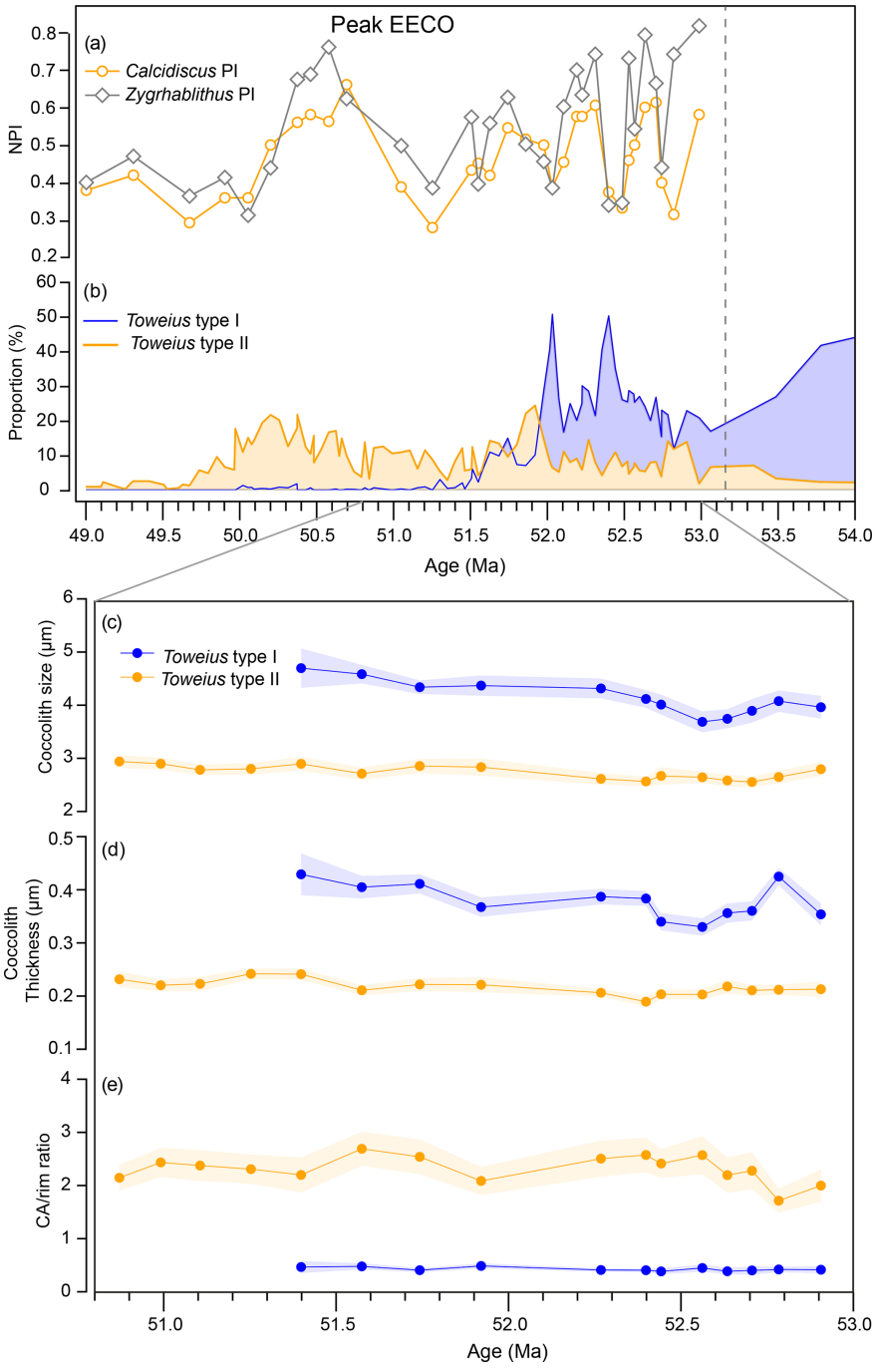

Figure 5. Time series of relative abundance and morphometric measurements of *Toweius* morphotypes. **(a)** *Calcidiscus*- and *Zygrhablithus*-based nannofossil preservation indices. **(b)** Relative abundance trend of *Toweius* types I and II. Temporal trends in **(c)** coccolith size, **(d)** thickness, and **(e)** central-area-to-rim ratio. Nannofossil preservation indices and relative abundance data are from Asanbe and Henderiks (2025).

plicates detailed species-level assessment of *Toweius* type I but is primarily restricted to fragile structures that are rarely preserved. Assessing the role of dissolution in the emergence of *Toweius* type II is more challenging, as the absence of both the central area and the inner tube would require a more severe and selective form of etching. If the R units of *Toweius* coccolith architecture were more susceptible to dissolution than the V units, we would expect to observe varying degrees of selective inner-tube removal in *Toweius* type I.

Compared to Site 865, where *Toweius* specimens exhibit signs of intense etching and breakage (Bralower and Mutterlose, 1995), LM and morphometric analyses at Site 1258 do

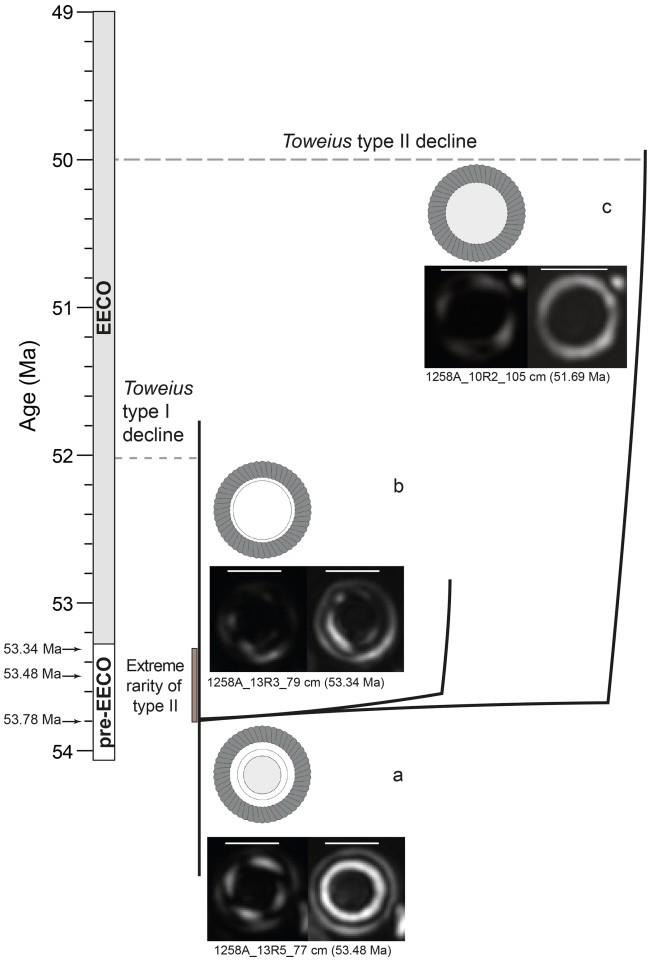

Figure 6. Proposed evolutionary trajectory of *Toweius* type II from *Toweius*. **(a)** Typical circular *Toweius* species. **(b)** A possible intermediate form and **(c)** *Toweius* type II, also observed in samples before the EECO. The black arrows indicate analyzed samples (range shown in the brown bar) before the EECO, where *Toweius* type II and likely intermediate forms occur. See Fig. 5b for the relative proportion of *Toweius* types I and II before the EECO. Scale bars equal 2 µm.

not show evidence of selective alteration of *Toweius* type I inner tubes or central opening diameters (Plate 1). For selective dissolution to account for the absence of the inner tube in *Toweius* type II, its precursor species would need to have possessed an inner tube as fragile and thin as the central area structures. This would imply that the dominant *Toweius* morphotype during peak EECO (52–50 Ma) evolved independently from pre-existing *Toweius* lineages that likely possessed thinner and more fragile inner tubes (Fig. 2a). The presence of rare transitional forms with thinner inner tubes in samples before the EECO supports the notion that *Toweius* type II may have emerged from species with inherently delicate inner tubes through mechanisms other than dissolution (Fig. 6).

Although dissolution may have obscured delicate structures in *Toweius* specimens, and possibly the fragile inner cycle of transitional *Toweius* type II forms, we argue that the evolutionary development of this more fragile inner cycle itself represents compelling evidence for phyletic speciation – a phenomenon that cannot be attributed solely to dissolution effects. Following this reasoning, we propose that the evolutionary pathway of *Toweius* type II involved either a gradual modification of intermediate forms with delicate inner cycles or a direct derivation from (sub)circular *Toweius* ancestors prior to the EECO (Fig. 6).

4.3 Stress-induced morphology versus true evolutionary speciation

Morphologically, the lightly calcified nature of *Toweius* type II could be directly related to structural abnormalities (malformation) during coccolithogenesis in response to environmental stress. Numerous experimental studies (e.g., Langer et al., 2011; Gerecht et al., 2014; Faucher et al., 2020) have shown that coccolithophores can produce abnormal coccolith morphologies as a physiological response to adverse physiochemical conditions outside their optimal growth ranges. Various cases of coccolith (and foraminifer) malformation have been reported in the fossil record in response to warming and carbonate undersaturation, particularly across the PETM, where extreme temperatures and elevated CO_2 levels exceeded that of the EECO. The PETM is notably marked by the widespread occurrence of transient excursion taxa (Kelly et al., 1996; Bralower, 2002; Kahn and Aubry, 2004; Raffi et al., 2005; Agnini et al., 2006, 2007), which typically disappear once environmental conditions stabilize. Despite large differences in temporal (and spatial) scales, such patterns may be consistent with malformation-induced morphologies observed in culture experiments, where normal coccolith formation resumes after environmental stress subsides. In contrast, our findings indicate that *Toweius* type II appeared before the EECO and that it persisted for more than 3 million years, far exceeding the duration of transient malformations recorded during the PETM. This prolonged presence suggests that *Toweius* type II represents a stable evolutionary lineage rather than a short-lived ecological stress response, supporting its interpretation as a product of true speciation rather than an environmentally induced phenotype or malformation. Based on this interpretation, *Toweius* type II warrants a formal taxonomic placement as a new species within *Toweius* (see Appendix), representing an evolutionary line extending from *Prinsius* through *Toweius* (likely *T. rotundus*; see nannotax).

4.4 Ecological and physiological significance of *Toweius* type II

The spatial and temporal distribution of *Toweius* type II underscores its ecological and physiological significance. This

morphotype is predominantly found in tropical regions, particularly in the equatorial Atlantic and Pacific, but is absent in other low-latitude deep-sea sites and well-preserved material from the Tanzania Drilling Project. This absence suggests that *Toweius* type II may have been confined to specific environmental conditions present in pelagic, near-equatorial regions. Given this biogeographical restriction, we posit that *Toweius* type II may be a tropical phenomenon, potentially shaped by distinct ecological constraints such as temperature, water column structure, or nutrient availability, which might have influenced its evolutionary trajectory during the early Eocene. While previous studies of *Toweius* have often generalized ecological preferences at the genus level, the genus exhibits broad morphological and genetic variation (Bown, 2010), indicating that individual species likely occupied diverse ecological niches. Self-Trail et al. (2012) show that species such as *T. serotinus*, *T. callosus*, and *T. occultatus* preferred warmer waters, while *T. eminens* and *T. tovae* favored cooler environments. On this basis, one could argue that *Toweius* phenotypical varieties are underpinned by species-specific physiological adaptation and ecological tolerance along biogeographical and environmental gradients.

Our study reveals that all the species represented in *Toweius* type I (known *Toweius* species) underwent an abrupt decline during the peak phase of EECO warming (Fig. 4b). The multi-million-year scale of this warming event – approximately 40 times longer in duration than the PETM – suggests that the physiological and ecological thresholds of *Toweius* type I were exceeded in the tropics. Previous studies concluded that heat stress and widespread oligotrophy likely acted as primary drivers, preventing any recovery (e.g., Agnini et al., 2006; Schneider et al., 2011; Asanbe and Henderiks, 2025). In contrast, *Toweius* type II persisted for an additional 2 million years, meaning that these two *Toweius* morphotypes show distinct ecological tolerance, with the peak EECO interval representing a critical warm and oligotrophic threshold. Combined, the inherently smaller coccolith size, thickness, and mass of *Toweius* type II suggest that overall lighter calcification may have been better suited to EECO conditions.

However, the emergence of *Toweius* type II before the EECO renders the hypothesis of a temporary physiological response or trait adaptation to environmental stress unlikely. Therefore, we propose that the abundance pattern of *Toweius* across the peak EECO is underpinned by morphotype selection related to (latitudinally controlled) environmental factors. Several observations from both modern ecosystems and the fossil record indicate that population shifts in *Emiliania huxleyi* morphotypes with varying degrees of calcification are driven by morphotype selection (Triantaphyllou et al., 2010; Beaufort et al., 2011; Meier et al., 2014a). As with taxonomic changes, these studies show that the turnover between heavier or lighter calcified morphotypes occurs in response to environmental changes and selection rather than through direct morphological alterations within existing species or morphotypes. It is, however, important to note that there is no consensus on how selective pressures favor differently calcified species/morphotypes in response to ocean chemistry, and no direct relationship has been established with other environmental parameters such as temperature and nutrient availability (Meier et al., 2014b; McClelland et al., 2016). Given the high CO_2 levels, prolonged warming, and low-nutrient conditions that characterized the peak EECO, it is plausible that reduced calcification in *Toweius* type II was underpinned by genetic regulation and associated with specific physiological adaptations. Because these adaptations may not be consistent in other lightly calcified species, we interpret this phenomenon as a taxon-specific ecological and physiological adaptation (Bolton and Stoll, 2013; Bach et al., 2015).

Beyond the degree of calcification, the large central-area-to-rim ratio – a defining characteristic of *Toweius* type II – also likely represents a form of ecological adaptation. This ratio is size independent and defines the extent of the central area, including regions occupied by pores, bars, or nets. Young (1987) proposed that the extent of central area opening may play a vital physiological role in cell–seawater interactions. This hypothesis was further described using an ecological model in a recent study (Ma et al., 2024), which proposed that a larger central opening may enhance nutrient uptake via mixotrophy. Although this model was applied to the adaptive morphology of large-celled *Reticulofenestra*, the enhanced nutrient acquisition central to this hypothesis might be relevant in explaining the prominence of small, relatively fast-growing species in stable oligotrophic environments. In the modern equatorial Pacific Ocean, medium-sized *Gephyrocapsa oceanica* with wide central areas are more abundant in stable oligotrophic environments than morphotypes with narrower central areas (Hagino et al., 2000). This indicates that the role of the central opening in ecological adaptation might be consistent across different nannoplankton species and morphotypes.

4.5 Early Eocene speciations in *Toweius*: *Toweius* type II and *Reticulofenestra* links

Our study demonstrates that the evolutionary emergence of novel morphotypes within the *Toweius* lineage occurred in the early Eocene, prior to the EECO. In a broader context of evolution, the timing of the appearance of *Toweius* type II is comparable to the early Eocene speciation of *Reticulofenestra* from *Toweius* (Agnini et al., 2006; Schneider et al., 2011). However, the emergence of these two taxa occurred in distinct biogeographic settings. While *Toweius* type II has so far been reported only in the tropics, *Reticulofenestra* first appeared in the Southern Ocean before expanding northward (Schneider et al., 2011). In addition to their distinct biogeographic origins, these taxa exhibit contrasting patterns in coccolith element loss: *Reticulofenestra* lost the V unit, whereas *Toweius* type II lost the R unit. This pattern of structural

modifications suggests that *Toweius* likely underwent multiple evolutionary pathways during the early Eocene, with *Reticulofenestra* ultimately representing the most successful evolutionary adaptation. Throughout the Cenozoic, *Reticulofenestra* underwent repeated bursts of morphological diversification (e.g., Young, 1990; Bown et al., 2004; Henderiks, 2008; Bendif et al., 2019; Henderiks et al., 2022; Ma et al., 2024). In contrast, while the ecological prominence of *Toweius* type II in tropical regions suggests it was a true species with a specialized adaptation to EECO conditions, its possible latitudinal restriction and decline during the subsequent cooling interval indicate a narrow ecological tolerance that ultimately limited its long-term success.

5 Conclusions

Biometry delineates two distinct *Toweius* morphotypes (type I and type II) and establishes an objective framework for their separation based on size, shape, and the central area. Despite the limitations of estimating calcite thickness (and thus mass) of V units under polarized light microscopy, our results reveal that *Toweius* type II lacks the inner- and middle-tube cycles of R units and exhibits a consistently smaller size and lower mass index, suggesting a generally lower degree of calcification than *Toweius* type I. This lower degree of calcification, coupled with a larger central-area-to-rim ratio, may have supported the ecological success of *Toweius* type II over type I in the extremely warm and oligotrophic tropical oceans of the EECO. We further demonstrate that *Toweius* type II emerged before the EECO, through the loss of inner-tube R units in (sub)circular *Toweius* ancestors. When considering the evolution of another descendant taxon, *Reticulofenestra*, which is marked by the loss of V units in *Toweius* ancestors, our findings indicate that the evolutionary trajectory of *Toweius* during the early Eocene was more diverse and complex than previously thought.

Appendix A

Systematic paleontological description of new *Toweius* species (referred to as *Toweius* type II above).

Family **Prinsiaceae** Hay and Mohler, 1967 emend. Young and Bown, 1997

Genus *Toweius* Hay and Mohler, 1967

Toweius tenuirotundus sp. nov
Plate 2, figs. 1–14

Derivation of name. Named for its distinctly thin, circular coccolith morphology, from the Latin adjective word *tenuis*, meaning "thin, slender", and *rotundus*, meaning "circular, round". The epithet *tenuirotundus* is formed as a compound adjective and agrees with the (masculine) genus *Toweius*.

Diagnosis. A small and thin, circular ring-like species of *Toweius* with an open central area and a complete absence of the R unit.

Description. This species is characterized by its small size ($\sim 3\,\mu m$) and thin, circular ring-like coccolith morphology. The coccolith is composed solely of the outer-tube cycle, which is characterized by curly and two lens-shaped extinction points on the coccolith rim under XPL. At 35° rotation under a crossed polarizer, these lens-shaped extinction points migrate along the rim (Plate 2, figs. 1a, b). Under SEM, the species exhibits the typical sinistral obliquity of the distal shield elements observed in other *Toweius* species. Both the distal and the proximal shields are well developed and structurally intact (Plate 2, figs. 3–8).

Differentiation. The species is readily distinguished from other *Toweius* species by the complete absence of R units and by the presence of two prominent lenticular extinction patterns along the coccolith rim. The sinistral obliquity of the distal shield elements further differentiates it from members of the *Coccolithaceae*, which characteristically exhibit dextral obliquity (dextral imbrication; Young, 1992). In addition, it can be distinguished from any members of the *Umbilicosphaera* genus by its non-birefringent appearance and curly rim bearing two lens-shaped extinction points under XPL.

Holotype. Plate 2, figs. 1a-c. Slide 207-1258A-10R-2, 105 cm, England Finder coordinate J42-4 (bordering K42-2; see also Supplement Table S4).

Holotype size. Length: 2.09 µm, width: 1.83 µm

Paratypes. Plate 2, figs. 2–14.

Dimensions. Based on biometric measurements of 842 specimens in 16 samples: coccolith length (L) of 2.08–4.41 µm (mean = 2.73 µm; SD = 0.30; variance = 0.09); coccolith width (W) of 1.69–3.70 µm (mean = 2.46 µm; SD = 0.27; variance = 0.07).

Type locality. The holotype and paratypes are designated from the equatorial Atlantic at ODP Leg 207, Site 1258, Hole A (Demerara Rise, coordinates: 9°26′ N, 54°43.9′ W; water depth 3192 m b.s.l.)

Type level. Early Eocene, calcareous nannofossil biozone NP12 (magnetochron C23n.2n) in deep-sea sediment sample ODP 207-1258A-10R2, 105 cm (79.9 m b.s.f.; 51.7 Ma).

Range. The observed stratigraphic range extends from the upper part of NP11 through to NP13 (Martini, 1971), corresponding to magnetochrons C24r to C21n. The depth interval is between 20.9 and 111.7 rmcd (corresponding to 54.3–46.2 Ma; cf. Westerhold et al., 2017) in ODP Site 1258, Hole A.

Occurrence. This species was particularly abundant during the EECO, reaching up to $\sim 20\,\%$ of the total nannofossil assemblage at ODP Site 1258. Abundance declined after ~ 50 Ma, after which the species became rare. This species has also been documented at ODP Site 865, in the equatorial Pacific (Asanbe and Henderiks, 2025; Bralower and Mutterlose, 1995).

Repository. The holotype and paratypes are archived at the Department of Earth Sciences, Uppsala University (reference slide ID: 207-1258A-10R2, 105 cm). Registration date: 4 March 2026, publication LSID: urn:lsid:zoobank.org:pub:BC4CF644-62FC-452C-901C-50C33A62DBF1, *Toweius tenuirotundus* LSID: urn:lsid:zoobank.org:act:7DBB2C6C-20B1-4458-962E-06A620CFC2B1.

Data availability. Additional data figures and tables are provided in the Supplement. The raw data produced for this paper are publicly available at the Zenodo data repository (https://doi.org/10.5281/zenodo.17201433, Asanbe and Henderiks, 2026).

Sample availability. The sediment samples and prepared microscope slides containing the calcareous nannofossils related to this study are archived at the Department of Earth Sciences, Uppsala University (Uppsala, Sweden).

Supplement. The supplement related to this article is available online at https://doi.org/10.5194/jm-45-159-2026-supplement.

Author contributions. Both authors (JDA and JH) conceived the study, designed the research hypotheses, and contributed to discussions and the interpretation of the results. JDA carried out sample analysis and microscopy and drafted the paper with contributions from JH. JDA and JH prepared and revised the figures.

Competing interests. The contact author has declared that neither of the authors has any competing interests.

Disclaimer. Publisher's note: Copernicus Publications remains neutral with regard to jurisdictional claims made in the text, published maps, institutional affiliations, or any other geographical representation in this paper. The authors bear the ultimate responsibility for providing appropriate place names. Views expressed in the text are those of the authors and do not necessarily reflect the views of the publisher.

Acknowledgements. The authors are grateful to the International Ocean Discovery Program (IODP) and the staff members at the Bremen Core Repository (Bremen University) and Gulf Coast Repository (Texas AandM University) for providing the deep-sea sediment samples for this research. This research was funded by Uppsala University and the Swedish Research Council under VR grant 2023-03719 awarded to JH. We thank Masayuki Utsunomiya and Jeremy Young for their constructive feedback, which helped improve the quality of this paper.

Financial support. This research has been supported by the Vetenskapsrådet (grant no. 2023-03719).

Review statement. This paper was edited by Juan Pablo Pérez Panera and reviewed by Masayuki Utsunomiya and Jeremy Young.

References

Agnini, C., Muttoni, G., Kent, D. V., and Rio, D.: Eocene biostratigraphy and magnetic stratigraphy from Possagno, Italy: The calcareous nannofossil response to climate variability, Earth Planet. Sc. Lett., 241, 815–830, https://doi.org/10.1016/j.epsl.2005.11.005, 2006.

Agnini, C., Fornaciari, E., Rio, D., Tateo, F., Backman, J., and Giusberti, L.: Responses of calcareous nannofossil assemblages, mineralogy and geochemistry to the environmental perturbations across the Paleocene/Eocene boundary in the Venetian Pre-Alps, Mar. Micropaleontol., 63, 19–38, https://doi.org/10.1016/j.marmicro.2006.10.002, 2007.

Alegret, L., Harper, D. T., Agnini, C., Newsam, C., Westerhold, T., Cramwinckel, M. J., Dallanave, E., Dickens, G. R., and Sutherland, R.: Biotic response to early Eocene warming events: Integrated record from Offshore Zealandia, North Tasman Sea, Paleoceanogr. Paleoclimatol., 36, https://doi.org/10.1029/2020PA004179, 2021.

Asanbe, J. D. and Henderiks, J.: Major Shifts in Equatorial Atlantic and Pacific Calcareous Nannofossil Assemblages Across the Early Eocene Climatic Optimum (EECO; ∼53–49 Ma), Paleoceanogr. Paleoclimatol., 40, e2024PA005038, https://doi.org/10.1029/2024PA005038, 2025.

Asanbe, J. and Henderiks, J.: Early Eocene evolutionary trajectories of within the Toweius genus: Insights from a newly identified species in the equatorial Atlantic – Coccolith biometric dataset, Zenodo [data set], https://doi.org/10.5281/zenodo.17201433, 2026.

Bach, L. T., Riebesell, U., Gutowska, M. A., Federwisch, L., and Schulz, K. G.: A unifying concept of coccolithophore sensitivity to changing carbonate chemistry embedded in an ecological framework, Prog. Oceanogr., 135, 125–138, https://doi.org/10.1016/j.pocean.2015.04.012, 2015.

Beaufort, L.: Weight estimates of coccoliths using the optical properties (birefringence) of calcite, Micropaleontology, 51, 289–297, https://doi.org/10.2113/gsmicropal.51.4.289, 2005.

Beaufort, L., Probert, I., de Garidel-Thoron, T., Bendif, E. M., Ruiz-Pino, D., Metzl, N., Goyet, C., Buchet, N., Coupel, P., Grelaud, M., Rost, B., Rickaby, R. E. M., and de Vargas, C.: Sensitivity of coccolithophores to carbonate chemistry and ocean acidification, Nature, 476, 80–83, https://doi.org/10.1038/nature10295, 2011.

Beaufort, L., Barbarin, N., and Gally, Y.: Optical measurements to determine the thickness of calcite crystals and the mass of thin carbonate particles such as coccoliths, Nat. Protoc., 9, 633–642, https://doi.org/10.1038/nprot.2014.028, 2014.

Beaufort, L., Gally, Y., Suchéras-Marx, B., Ferrand, P., and Dubois-set, J.: Technical note: A universal method for measuring the thickness of microscopic calcite crystals, based on bidirectional circular polarization, Biogeosciences, 18, 775–785, https://doi.org/10.5194/bg-18-775-2021, 2021.

Bendif, E. M., Nevado, B., Wong, E. L. Y., Hagino, K., Probert, I., Young, J. R., Rickaby, R. E. M., and Filatov, D. A.: Repeated species radiations in the recent evolution of the key marine phytoplankton lineage *Gephyrocapsa*, Nat. Commun., 10, 4234, https://doi.org/10.1038/s41467-019-12169-7, 2019.

Bolton, C. T. and Stoll, H. M.: Late Miocene threshold response of marine algae to carbon dioxide limitation, Nature, 500, 558–562, https://doi.org/10.1038/nature12448, 2013.

Bordiga, M., Bartol, M., and Henderiks, J.: Absolute nannofossil abundance estimates: Quantifying the pros and cons of different techniques, Revue de Micropaléontologie, 58, 155–165, https://doi.org/10.1016/j.revmic.2015.05.002, 2015.

Bown, P. and Pearson, P.: Calcareous plankton evolution and the Paleocene/Eocene thermal maximum event: New evidence from Tanzania, Mar. Micropaleontol., 71, 60–70, https://doi.org/10.1016/j.marmicro.2009.01.005, 2009.

Bown, P. R.: Calcareous nannofossils from the Paleocene/Eocene Thermal Maximum interval of southern Tanzania (TDP Site 14), International Nannoplankton Association, 31, 11–38, 2010.

Bown, P. R., Lees, J. A., and Young, J. R.: Calcareous nannoplankton evolution and diversity through time, in: Coccolithophores, edited by: Thierstein, H. R. and Young, J. R., Springer Berlin Heidelberg, Berlin, Heidelberg, 481–508, https://doi.org/10.1007/978-3-662-06278-4_18, 2004.

Bown, P. R., Jones, T. D., Lees, J. A., Randell, R. D., Mizzi, J. A., Pearson, P. N., Coxall, H. K., Young, J. R., Nicholas, C. J., Karega, A., Singano, J., and Wade, B. S.: A Paleogene calcareous microfossil Konservat-Lagerstatte from the Kilwa Group of coastal Tanzania, Geol. Soc. Am. Bull., 120, 3–12, https://doi.org/10.1130/B26261.1, 2008.

Bown, P. R., Kim, H., and Gibbs, S. J.: Danian calcareous nannofossil evolution and taxonomy with focus on sites from the North Atlantic Ocean (IODP Expedition 342, Sites U1403 and U1407), J. Nannoplankton Res., 41, 110–157, https://doi.org/10.58998/jnr3943, 2023.

Bralower, T. J.: Evidence of surface water oligotrophy during the Paleocene-Eocene thermal maximum: Nannofossil assemblage data from Ocean Drilling Program Site 690, Maud Rise, Weddell Sea, Paleoceanography, 17, https://doi.org/10.1029/2001PA000662, 2002.

Bralower, T. J. and Mutterlose, J.: Calcareous nannofossil biostratigraphy of Site 865, Allison Guyot, central Pacific Ocean: A tropical Paleogene reference section, in: Proceedings of the Ocean Drilling Program, Scientific Results, vol. 143, Ocean Drilling Program, College Station, https://doi.org/10.2973/odp.proc.sr.143.204.1995, 1995.

Cappelli, C., Bown, P. R., Westerhold, T., Bohaty, S. M., Riu, M., Lobba, V., Yamamoto, Y., and Agnini, C.: The early to middle Eocene transition: An integrated calcareous nannofossil and stable isotope record from the Northwest Atlantic Ocean (Integrated Ocean Drilling Program Site U1410), Paleoceanogr. Paleoclimatol.,, 34, 1913–1930, https://doi.org/10.1029/2019PA003686, 2019.

Cubillos, J. C., Henderiks, J., Beaufort, L., Howard, W. R., and Hallegraeff, G. M.: Reconstructing calcification in ancient coccolithophores: Individual coccolith weight and morphology of *Coccolithus pelagicus* (sensu lato), Mar. Micropaleontol., 92–93, 29–39, https://doi.org/10.1016/j.marmicro.2012.04.005, 2012.

Dunkley Jones, T., Bown, P. R., Pearson, P. N., Wade, B. S., Coxall, H. K., and Lear, C. H.: Major shifts in calcareous phytoplankton assemblages through the Eocene-Oligocene transition of Tanzania and their implications for low-latitude primary production, Paleoceanography, 23, 2008PA001640, https://doi.org/10.1029/2008PA001640, 2008.

Erbacher, J., Mosher, D. C., Malone, M. J., Sexton, P., and Wilson, P. A. (Eds.): Proceedings of the Ocean Drilling Program, 207 Initial Reports, Ocean Drilling Program, https://doi.org/10.2973/odp.proc.ir.207.2004, 2004.

Faucher, G., Riebesell, U., and Bach, L. T.: Can morphological features of coccolithophores serve as a reliable proxy to reconstruct environmental conditions of the past?, Clim. Past, 16, 1007–1025, https://doi.org/10.5194/cp-16-1007-2020, 2020.

Gerecht, A. C., Šupraha, L., Edvardsen, B., Probert, I., and Henderiks, J.: High temperature decreases the PIC / POC ratio and increases phosphorus requirements in Coccolithus pelagicus (Haptophyta), Biogeosciences, 11, 3531–3545, https://doi.org/10.5194/bg-11-3531-2014, 2014.

Gibbs, S. J., Bown, P. R., Sessa, J. A., Bralower, T. J., and Wilson, P. A.: Nannoplankton extinction and origination across the Paleocene-Eocene Thermal Maximum, Science, 314, 1770–1773, https://doi.org/10.1126/science.1133902, 2006.

Gibbs, S. J., Sheward, R. M., Bown, P. R., Poulton, A. J., and Alvarez, S. A.: Warm plankton soup and red herrings: calcareous nannoplankton cellular communities and the Palaeocene–Eocene Thermal Maximum, Phil. Trans. R. Soc. A., 376, 20170075, https://doi.org/10.1098/rsta.2017.0075, 2018.

Hagino, K., Okada, H., and Matsuoka, H.: Spatial dynamics of coccolithophore assemblages in the Equatorial Western-Central Pacific Ocean, Mar. Micropaleontol., 39, 53–72, https://doi.org/10.1016/S0377-8398(00)00014-1, 2000.

Haq, B. U. and Lohmann, G. P.: Early Cenozoic calcareous nannoplankton biogeography of the Atlantic Ocean, Mar. Micropaleontol., 1, 119–194, https://doi.org/10.1016/0377-8398(76)90008-6, 1976.

Hay, W. W. and Mohler, H. P.: Calcareous nannoplankton from early Tertiary rocks at Pont Labau, France, and Paleocene-early Eocene correlations, Journal of Paleontology, 41, 1505–1541, 1967.

Henderiks, J.: Coccolithophore size rules – Reconstructing ancient cell geometry and cellular calcite quota from fossil coccoliths, Mar. Micropaleontol., 67, 143–154, https://doi.org/10.1016/j.marmicro.2008.01.005, 2008.

Henderiks, J., Sturm, D., Šupraha, L., and Langer, G.: Evolutionary Rates in the Haptophyta: Exploring Molecular and Phenotypic Diversity, J. Mar. Sci. Eng., 10, 798, https://doi.org/10.3390/jmse10060798, 2022.

Hollis, C. J., Handley, L., Crouch, E. M., Morgans, H. E. G., Baker, J. A., Creech, J., Collins, K. S., Gibbs, S. J., Huber, M., Schouten, S., Zachos, J. C., and Pancost, R. D.: Tropical sea temperatures in the high-latitude South Pacific during the Eocene, Geology, 37, 99–102, https://doi.org/10.1130/G25200A.1, 2009.

Hollis, C. J., Dunkley Jones, T., Anagnostou, E., Bijl, P. K., Cramwinckel, M. J., Cui, Y., Dickens, G. R., Edgar, K. M., Eley, Y., Evans, D., Foster, G. L., Frieling, J., Inglis, G. N., Kennedy, E. M., Kozdon, R., Lauretano, V., Lear, C. H., Littler, K., Lourens, L., Meckler, A. N., Naafs, B. D. A., Pälike, H., Pancost, R. D., Pearson, P. N., Röhl, U., Royer, D. L., Salz-

mann, U., Schubert, B. A., Seebeck, H., Sluijs, A., Speijer, R. P., Stassen, P., Tierney, J., Tripati, A., Wade, B., Westerhold, T., Witkowski, C., Zachos, J. C., Zhang, Y. G., Huber, M., and Lunt, D. J.: The DeepMIP contribution to PMIP4: methodologies for selection, compilation and analysis of latest Paleocene and early Eocene climate proxy data, incorporating version 0.1 of the DeepMIP database, Geosci. Model Dev., 12, 3149–3206, https://doi.org/10.5194/gmd-12-3149-2019, 2019.

Kahn, A. and Aubry, M.-P.: Provincialism associated with the Paleocene/Eocene thermal maximum: temporal constraint, Mar. Micropaleontol., 52, 117–131, https://doi.org/10.1016/j.marmicro.2004.04.003, 2004.

Kelly, D. C., Bralower, T. J., Zachos, J. C., Silva, I. P., and Thomas, E.: Rapid diversification of planktonic foraminifera in the tropical Pacific (ODP Site 865) during the late Paleocene thermal maximum, Geol., 24, 423, https://doi.org/10.1130/0091-7613(1996)024<0423:RDOPFI>2.3.CO;2, 1996.

Langer, G., Probert, I., Nehrke, G., and Ziveri, P.: The morphological response of *Emiliania huxleyi* to seawater carbonate chemistry changes: an inter-strain comparison, J. Nannoplankton Res., 32, 29–36, https://doi.org/10.58998/jnr2159, 2011.

Ma, R., Aubry, M.-P., Bord, D., Jin, X., and Liu, C.: Inferred nutrient forcing on the late middle Eocene to early Oligocene (∼ 40–31 Ma) evolution of the coccolithophore *Reticulofenestra* (order Isochrysidales), Paleobiology, 50, 29–42, https://doi.org/10.1017/pab.2023.20, 2024.

Martini, E.: Standard Tertiary and Quaternary calcareous nannoplankton zonation, in Proceedings of the Second Planktonic Conference Roma 1970, Edizioni Technoscienza, Rome, 2, 739–785, 1971.

Mather, B. R., Müller, R. D., Zahirovic, S., Cannon, J., Chin, M., Ilano, L., Wright, N. M., Alfonso, C., Williams, S., Tetley, M., and Merdith, A.: Deep time spatio-temporal data analysis using pyGPlates with Plate Tectonic Tools and GPlately, Geosci. Data J., 11, 3–10, https://doi.org/10.1002/gdj3.185, 2023.

McClelland, H. L. O., Barbarin, N., Beaufort, L., Hermoso, M., Ferretti, P., Greaves, M., and Rickaby, R. E. M.: Calcification response of a key phytoplankton family to millennial-scale environmental change, Sci. Rep., 6, 34263, https://doi.org/10.1038/srep34263, 2016.

Meier, K. J. S., Berger, C., and Kinkel, H.: Increasing coccolith calcification during CO_2 rise of the penultimate deglaciation (Termination II), Mar. Micropaleontol., 112, 1–12, https://doi.org/10.1016/j.marmicro.2014.07.001, 2014a.

Meier, K. J. S., Beaufort, L., Heussner, S., and Ziveri, P.: The role of ocean acidification in *Emiliania huxleyi* coccolith thinning in the Mediterranean Sea, Biogeosciences, 11, 2857–2869, https://doi.org/10.5194/bg-11-2857-2014, 2014b.

Müller, R. D., Cannon, J., Williams, S., and Dutkiewicz, A.: PyBacktrack 1.0: A Tool for Reconstructing Paleobathymetry on Oceanic and Continental Crust, Geochem. Geophy. Geosy., 19, 1898–1909, https://doi.org/10.1029/2017GC007313, 2018.

Müller, R. D., Zahirovic, S., Williams, S. E., Cannon, J., Seton, M., Bower, D. J., Tetley, M. G., Heine, C., Le Breton, E., Liu, S., Russell, S. H. J., Yang, T., Leonard, J., and Gurnis, M.: A global plate model including lithospheric deformation along major rifts and orogens since the Triassic, Tectonics, 38, 1884–1907, https://doi.org/10.1029/2018TC005462, 2019.

Mutterlose, J., Linnert, C., and Norris, R.: Calcareous nannofossils from the Paleocene–Eocene Thermal Maximum of the equatorial Atlantic (ODP Site 1260B): Evidence for tropical warming, Mar. Micropaleontol., 65, 13–31, https://doi.org/10.1016/j.marmicro.2007.05.004, 2007.

Pearson, P. N., McMillan, I. K., Wade, B. S., Jones, T. D., Coxall, H. K., Bown, P. R., and Lear, C. H.: Extinction and environmental change across the Eocene-Oligocene boundary in Tanzania, Geol., 36, 179, https://doi.org/10.1130/G24308A.1, 2008.

Raffi, I. and De Bernardi, B.: Response of calcareous nannofossils to the Paleocene–Eocene Thermal Maximum: Observations on composition, preservation and calcification in sediments from ODP Site 1263 (Walvis Ridge – SW Atlantic), Mar. Micropaleontol., 69, 119–138, https://doi.org/10.1016/j.marmicro.2008.07.002, 2008.

Raffi, I., Backman, J., and Pälike, H.: Changes in calcareous nannofossil assemblages across the Paleocene/Eocene transition from the paleo-equatorial Pacific Ocean, Palaeogeography, Palaeoclimatology, Palaeoecology, 226, 93–126, https://doi.org/10.1016/j.palaeo.2005.05.006, 2005.

Romein, A. J. T.: Evolutionary lineages in early Paleogene calcareous nannoplankton, Utrecht Micropaleontological Bulletins, 22, 1–230, 1979.

Roth, P. H.: Cretaceous nannoplankton biostratigraphy and oceanography of the Northwestern Atlantic Ocean, in: Initial reports of the Deep Sea Drilling Project; Volume XLIV covering Leg 44 of the cruises of the drilling vessel Glomar Challenger, Norfolk, 44, 731–759, https://doi.org/10.2973/dsdp.proc.44.134.1978, 1978.

Roth, P. H. and Thierstein, H. R.: Calcareous nannoplankton: Leg 14 of the Deep Sea Drilling Project, Init. Repts. DSDP, 14, 421–485, https://doi.org/10.2973/dsdp.proc.14.114.1972, 1972.

Schneider, L. J., Bralower, T. J., and Kump, L. R.: Response of nannoplankton to early Eocene ocean destratification, Palaeogeography, Palaeoclimatology, Palaeoecology, 310, 152–162, https://doi.org/10.1016/j.palaeo.2011.06.018, 2011.

Self-Trail, J. M., Powars, D. S., Watkins, D. K., and Wandless, G. A.: Calcareous nannofossil assemblage changes across the Paleocene–Eocene Thermal Maximum: Evidence from a shelf setting, Mar. Micropaleontol., 92–93, 61–80, https://doi.org/10.1016/j.marmicro.2012.05.003, 2012.

Shamrock, J. L. and Watkins, D. K.: Eocene calcareous nannofossil biostratigraphy and community structure from Exmouth Plateau, Eastern Indian Ocean (ODP Site 762), Stratigraphy, 9, https://doi.org/10.29041/strat.09.1.01, 2012.

Shepherd, C. L., Kulhanek, D. K., Hollis, C. J., Morgans, H. E. G., Strong, C. P., Pascher, K. M., and Zachos, J. C.: Calcareous nannoplankton response to early Eocene warmth, Southwest Pacific Ocean, Mar. Micropaleontol., 165, 101992, https://doi.org/10.1016/j.marmicro.2021.101992, 2021.

Sullivan, F. R.: Lower Tertiary Nannoplankton from the California Coast Ranges, University of California Press, ISBN 9780598201416, 1965.

Šupraha, L. and Henderiks, J.: A 15-million-year-long record of phenotypic evolution in the heavily calcified coccolithophore Helicosphaera and its biogeochemical implications, Biogeosciences, 17, 2955–2969, https://doi.org/10.5194/bg-17-2955-2020, 2020.

Triantaphyllou, M., Dimiza, M., Krasakopoulou, E., Malinverno, E., Lianou, V., and Souvermezoglou, E.: Seasonal variation in *Emiliania huxleyi* coccolith morphology and calcification in the Aegean Sea (Eastern Mediterranean), Geobios, 43, 99–110, https://doi.org/10.1016/j.geobios.2009.09.002, 2010.

Wei, W. and Wise, S. W.: Biogeographic gradients of middle Eocene-Oligocene calcareous nannoplankton in the South Atlantic Ocean, Palaeogeography, Palaeoclimatology, Palaeoecology, 79, 29–61, https://doi.org/10.1016/0031-0182(90)90104-F, 1990.

Westerhold, T. and Röhl, U.: High resolution cyclostratigraphy of the early Eocene – new insights into the origin of the Cenozoic cooling trend, Clim. Past, 5, 309–327, https://doi.org/10.5194/cp-5-309-2009, 2009.

Westerhold, T., Röhl, U., Frederichs, T., Agnini, C., Raffi, I., Zachos, J. C., and Wilkens, R. H.: Astronomical calibration of the Ypresian timescale: implications for seafloor spreading rates and the chaotic behavior of the solar system?, Clim. Past, 13, 1129–1152, https://doi.org/10.5194/cp-13-1129-2017, 2017.

Westerhold, T., Röhl, U., Donner, B., and Zachos, J. C.: Global extent of early Eocene hyperthermal events: A new Pacific benthic foraminiferal isotope record from Shatsky Rise (ODP Site 1209), Paleoceanogr. Paleoclimatol., 33, 626–642, https://doi.org/10.1029/2017PA003306, 2018.

Westerhold, T., Marwan, N., Drury, A. J., Liebrand, D., Agnini, C., Anagnostou, E., Barnet, J. S. K., Bohaty, S. M., De Vleeschouwer, D., Florindo, F., Frederichs, T., Hodell, D. A., Holbourn, A. E., Kroon, D., Lauretano, V., Littler, K., Lourens, L. J., Lyle, M., Pälike, H., Röhl, U., Tian, J., Wilkens, R. H., Wilson, P. A., and Zachos, J. C.: An astronomically dated record of Earth's climate and its predictability over the last 66 million years, Science, 369, 1383–1387, https://doi.org/10.1126/science.aba6853, 2020.

Young, J. R.: Possible functional interpretation of coccolith morphology, Geologische Bundesanstalt, 305–313, ISBN 3-900312-54-0, 1987.

Young, J. R.: Size variation of Neogene *Reticulofenestra* coccoliths from Indian Ocean DSDP Cores, J. Micropalaeontol., 9, 71–85, https://doi.org/10.1144/jm.9.1.71, 1990.

Young, J. R.: The description and analysis of coccolith structure, in: Proceedings of the 4th INA Conference, edited by: Hamrsmid, B. and Young, J. R., Prague, Knihovnicka ZPN, 14a, 35–71, 1992.

Young, J. R., Geisen, M., Cros, L., Kleijne, A., Probert, I., and Ostergaard, J. B.: A guide to extant coccolithophore taxonomy, J. Nannoplankton Res., S1, 1–132, https://doi.org/10.58998/jnr2297, 2003.

Young, J. R., Geisen, M., and Probert, I.: A review of selected aspects of coccolithophore biology with implications for paleobiodiversity estimation, Micropaleontology, 51, 267–288, https://doi.org/10.2113/gsmicropal.51.4.267, 2005.

Zachos, J., Pagani, M., Sloan, L., Thomas, E., and Billups, K.: Trends, Rhythms, and Aberrations in Global Climate 65 Ma to Present, Science, 292, 686–693, https://doi.org/10.1126/science.1059412, 2001.

Zachos, J. C., Dickens, G. R., and Zeebe, R. E.: An early Cenozoic perspective on greenhouse warming and carbon-cycle dynamics, Nature, 451, 279–283, https://doi.org/10.1038/nature06588, 2008.